



Supplement of

Slow feedbacks resulting from strongly enhanced atmospheric methane mixing ratios in a chemistry–climate model with mixed-layer ocean

Laura Stecher et al.

Correspondence to: Laura Stecher (laura.stecher@dlr.de)

The copyright of individual parts of the supplement might differ from the CC BY 4.0 License.

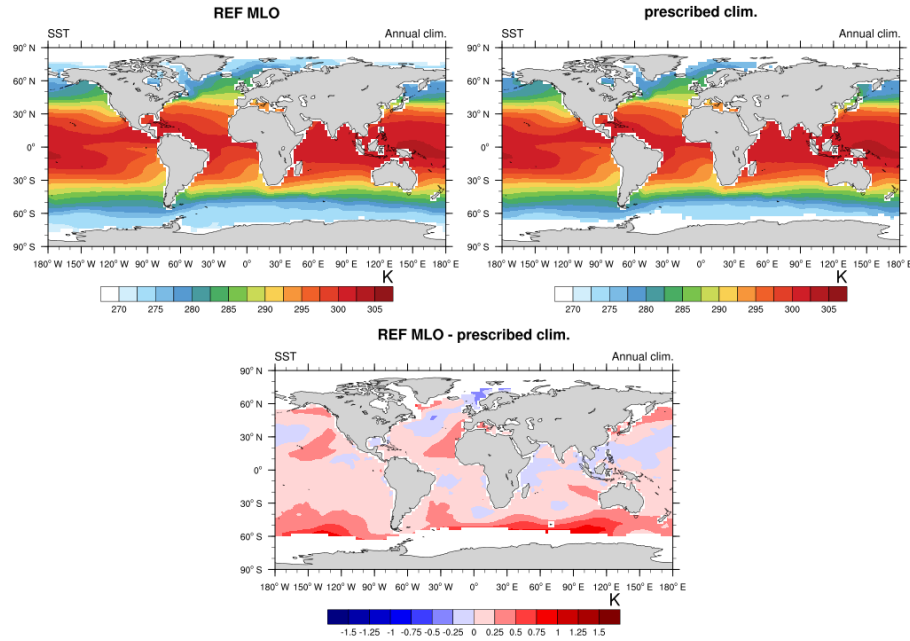


Figure S1. Climatologies of annual mean sea surface temperatures of REF MLO (top left) and the climatology (Rayner et al., 2003) prescribed as lower boundary for REF QFLX and REF fSST (top right), and their difference (bottom middle).

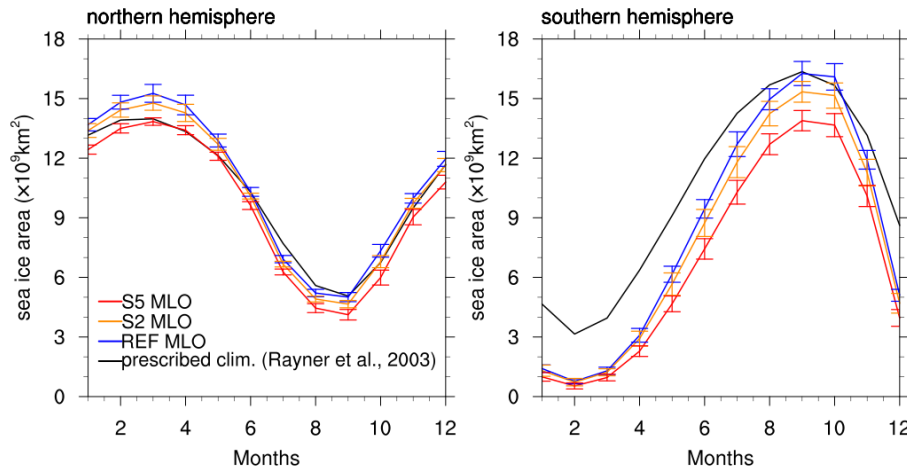


Figure S2. Monthly climatologies of total sea ice area in the Northern Hemisphere (left) and in the Southern Hemisphere (right) for REF MLO (blue), S2 MLO (orange), S5 MLO (red) and the prescribed climatology (black). For the MLO simulations the interannual standard deviations are indicated by vertical lines.

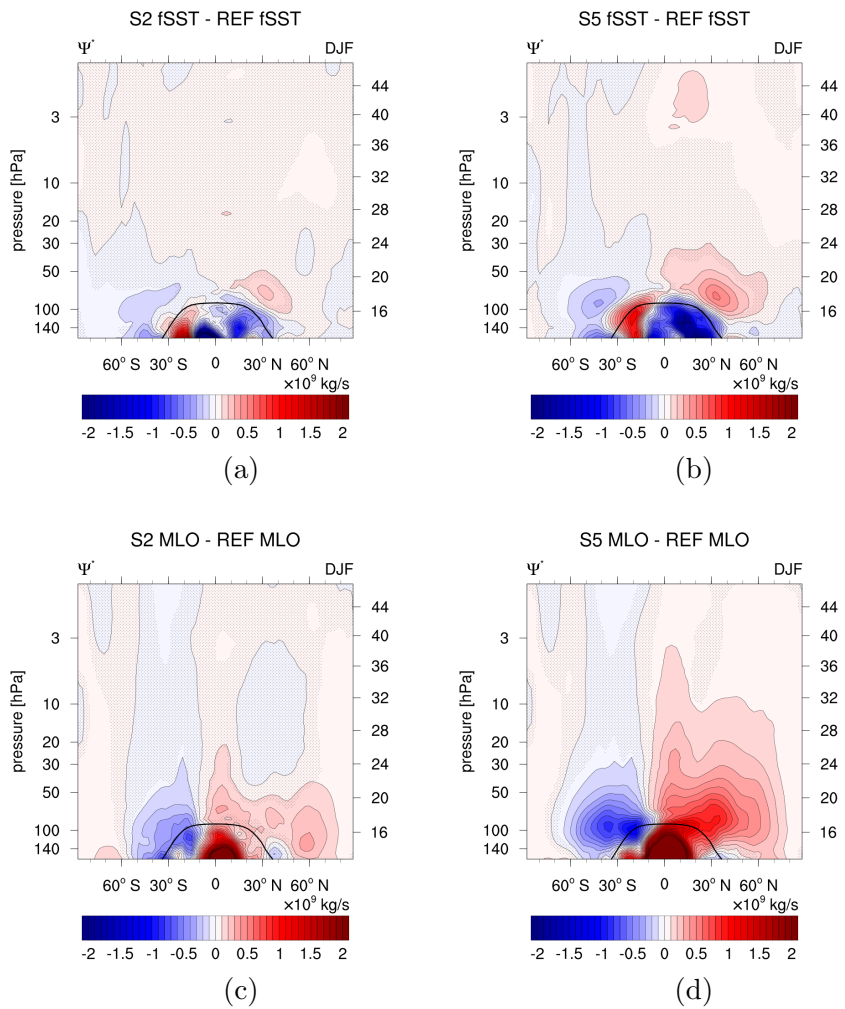


Figure S3. Absolute differences of the residual mean streamfunction for season December, January, and February (DJF) of the sensitivity simulations (a) S2 fSST, (b) S5 fSST, (c) S2 MLO, (d) S5 MLO and their respective reference in 10^9 kg s^{-1} . Non-stippled areas are significant on the 95 % confidence level according to a two sided Welch's test. The solid black line indicates the climatological tropopause height of REF MLO.

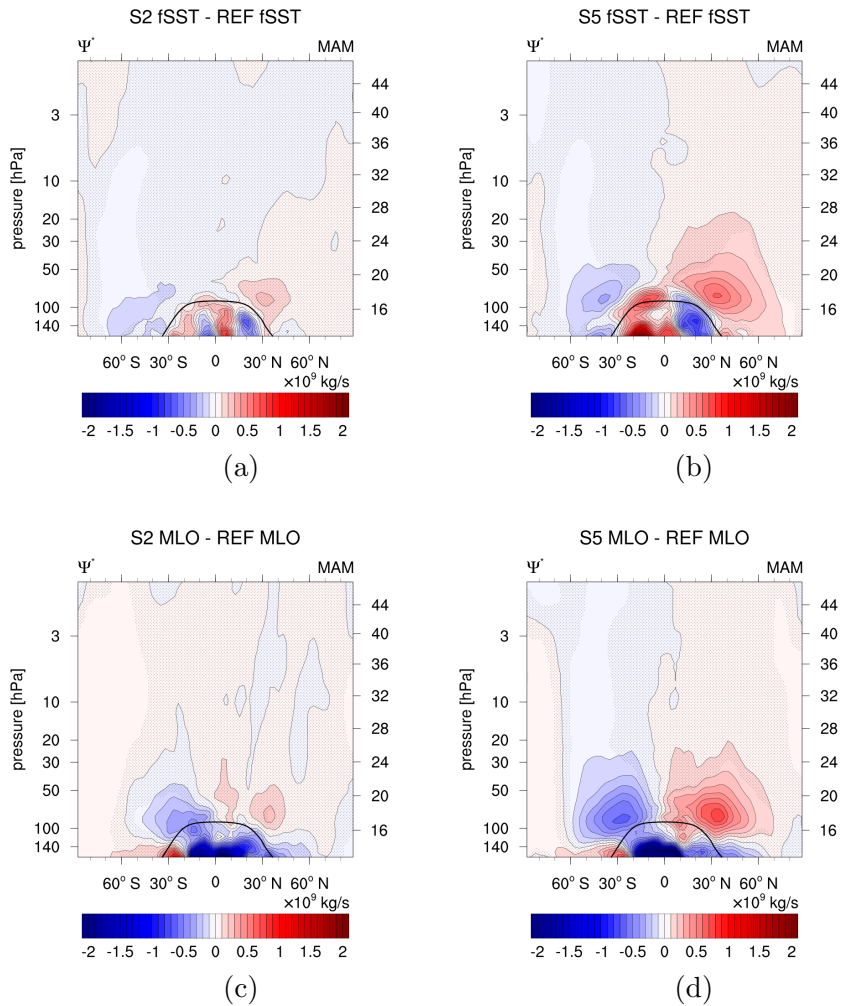


Figure S4. Absolute differences of the residual mean streamfunction for season March, April, and May (MAM) of the sensitivity simulations (a) S2 fSST, (b) S5 fSST, (c) S2 MLO, (d) S5 MLO and their respective reference in 10^9 kg s^{-1} . Non-stippled areas are significant on the 95 % confidence level according to a two sided Welch's test. The solid black line indicates the climatological tropopause height of REF MLO.

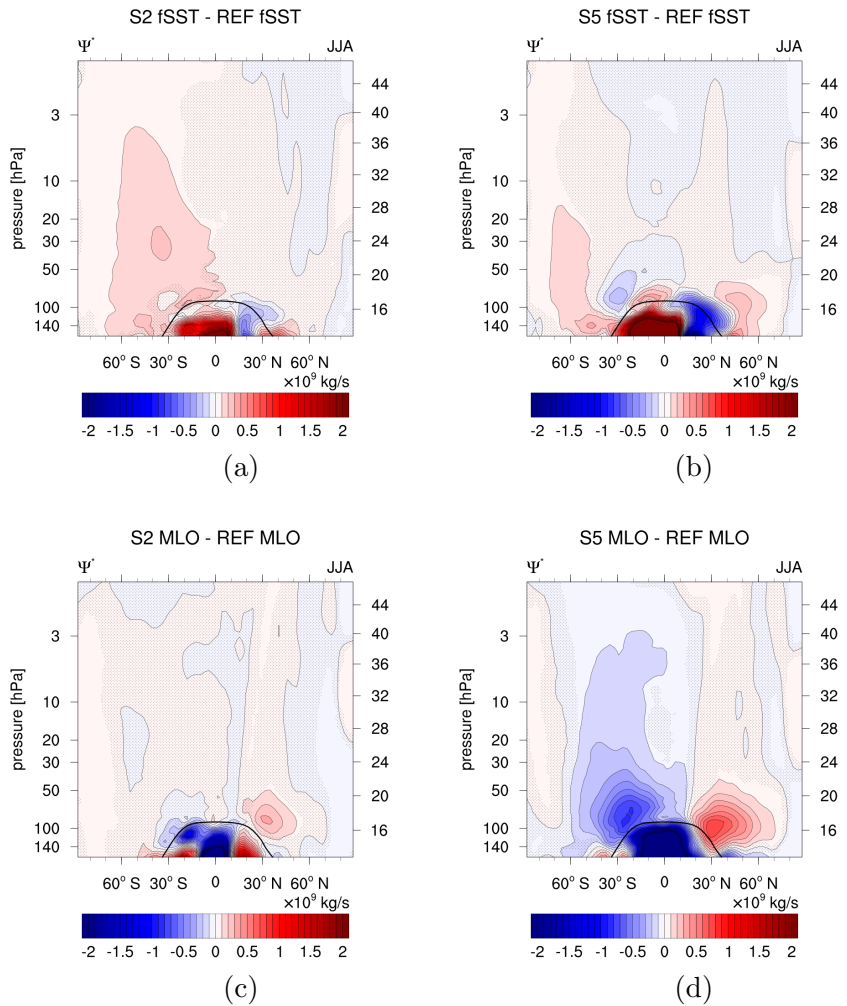


Figure S5. Absolute differences of the residual mean streamfunction for season June, July, and August (JJA) of the sensitivity simulations (a) S2 fSST, (b) S5 fSST, (c) S2 MLO, (d) S5 MLO and their respective reference in 10^9 kg s^{-1} . Non-stippled areas are significant on the 95 % confidence level according to a two sided Welch's test. The solid black line indicates the climatological tropopause height of REF MLO.

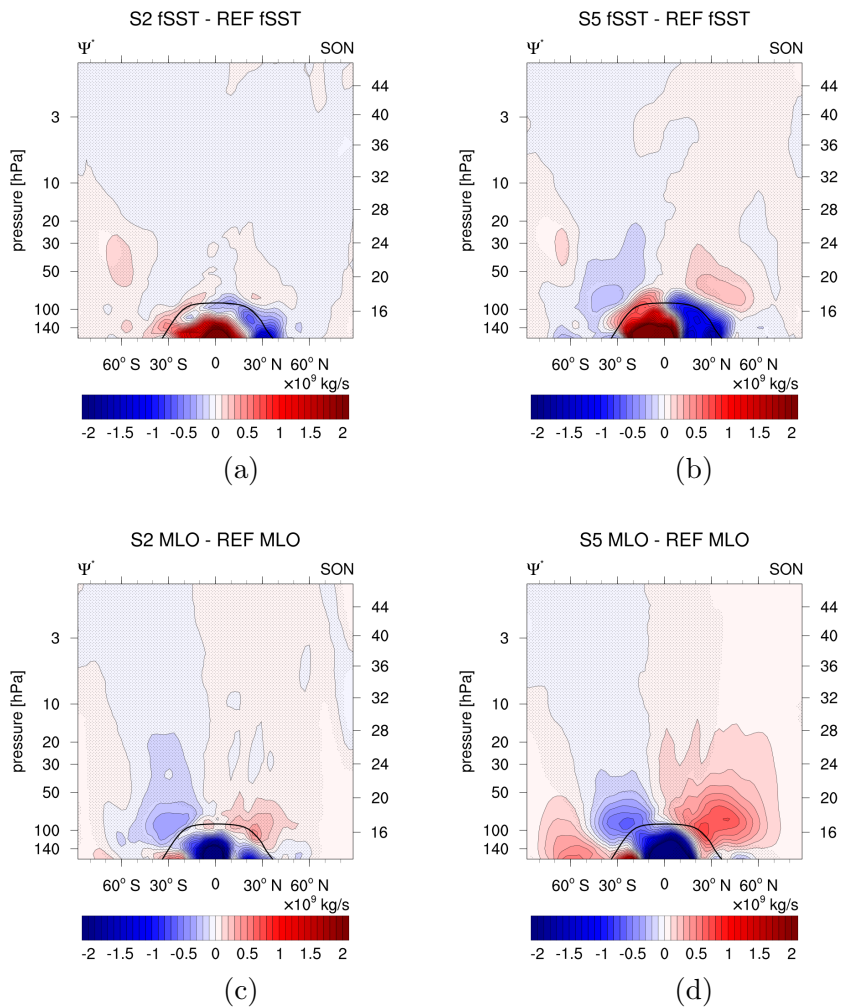


Figure S6. Absolute differences of the residual mean streamfunction for season September, October, and November (SON) of the sensitivity simulations (a) S2 fSST, (b) S5 fSST, (c) S2 MLO, (d) S5 MLO and their respective reference in 10^9 kg s^{-1} . Non-stippled areas are significant on the 95 % confidence level according to a two sided Welch's test. The solid black line indicates the climatological tropopause height of REF MLO.

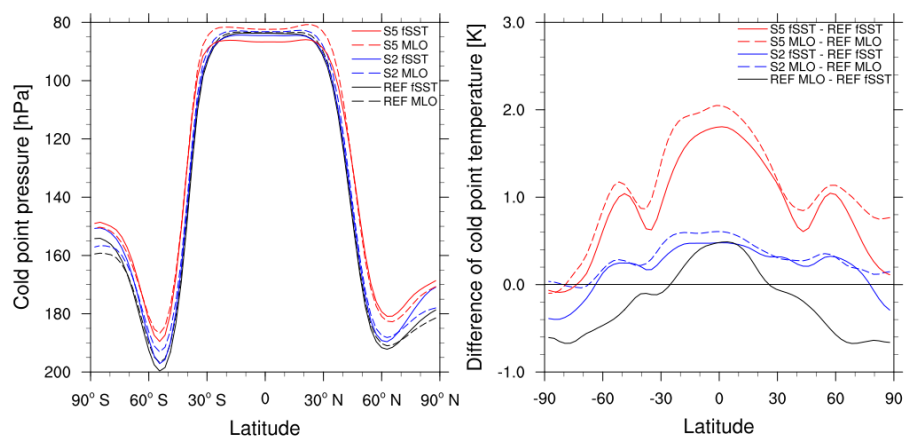


Figure S7. Left: Cold point pressure in hPa. Right: Difference of cold point temperature of the sensitivity simulations and their respective reference in K and difference of cold point temperature between REF MLO and REF fSST in K (black).

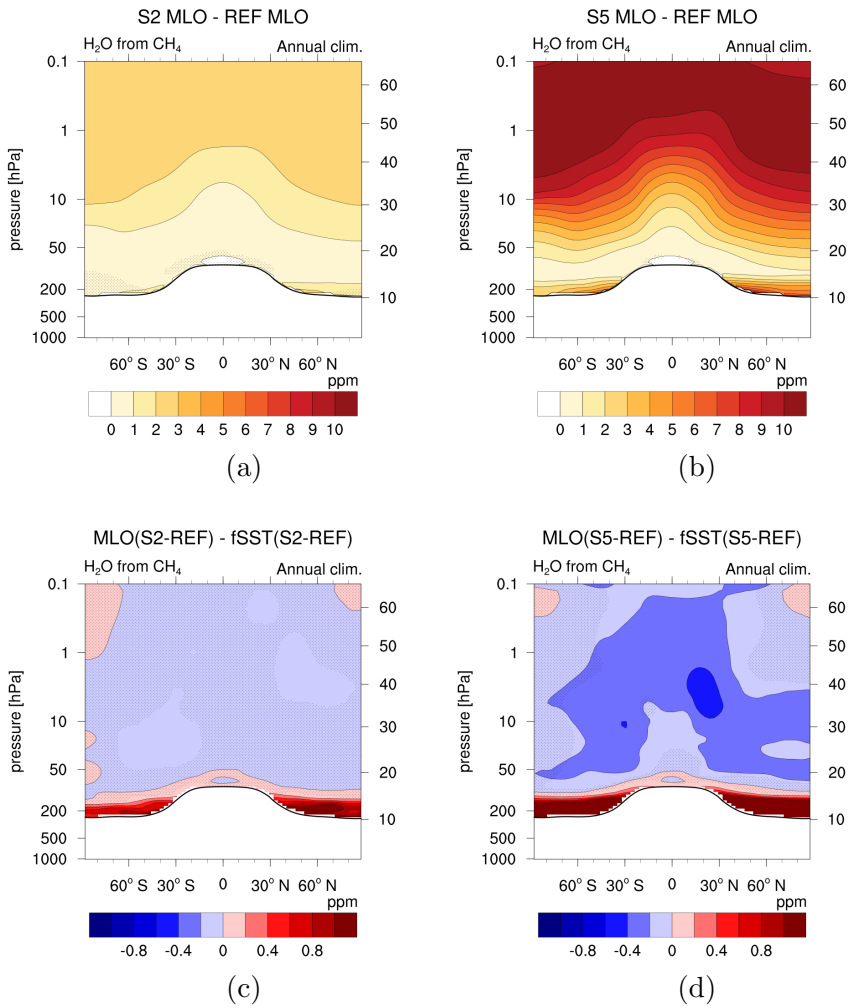


Figure S8. Upper row: Estimate of the differences of the annual zonal mean H₂O produced by CH₄ oxidation (H₂O_{CH₄}) between the sensitivity simulations (a) S2 MLO and (b) S5 MLO and REF MLO in ppm. Lower row: Differences between the H₂O_{CH₄} response in the MLO and fSST set-ups in ppm. H₂O from CH₄ is estimated as H₂O_{CH₄} = H₂O - H₂O_{entry}. Non-stippled areas are significant on the 95 % confidence level according to a two sided Welch's test. The solid black line indicates the climatological tropopause height of REF MLO.

$$\Delta T_{\text{adj}}(\text{S2}^* - \text{REF}^*)_{\text{MLO}}$$

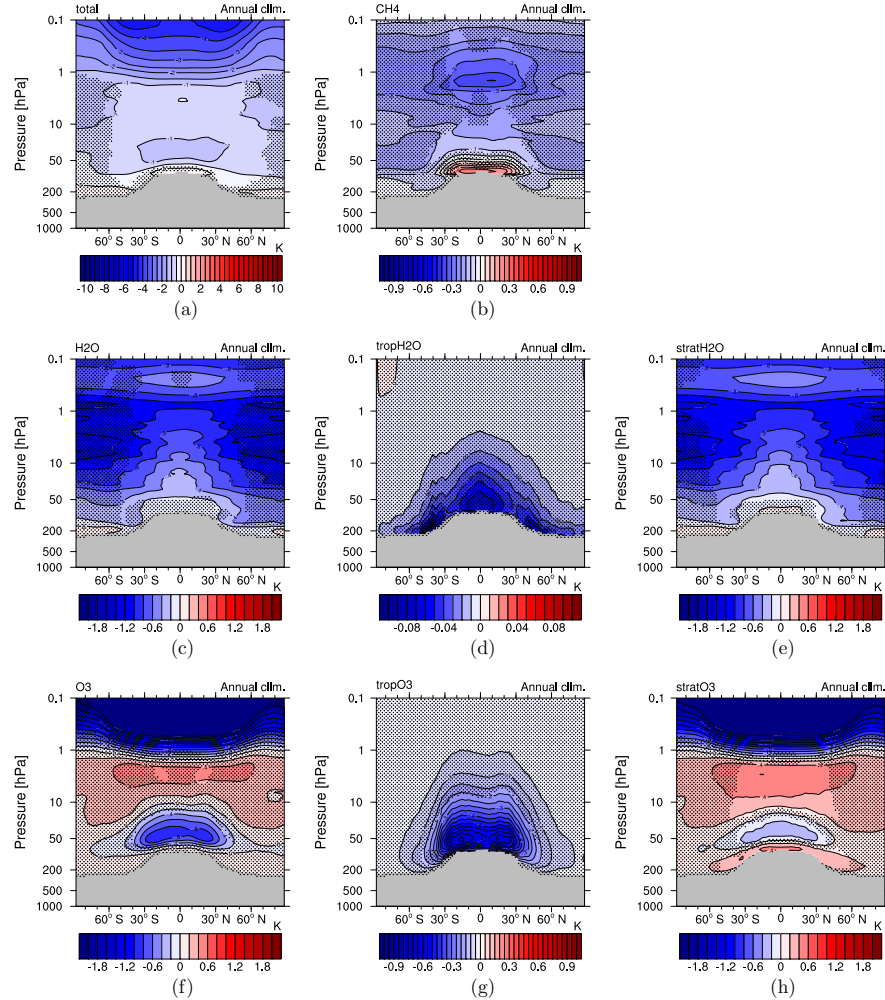


Figure S9. Stratospheric temperature adjustment radiatively induced by individual species changes in simulation S2 MLO ($2\times\text{CH}_4$): (a) CH_4 , H_2O and O_3 combined, (b) CH_4 , (c) H_2O , (d) tropospheric H_2O only, (e) stratospheric H_2O only (SWV), (f) O_3 , (g) tropospheric O_3 only and (h) stratospheric O_3 only. Note the different colour bars in panels (a), (b), (d) and (g).

$$\Delta T_{\text{adj}}(\text{S2}^* - \text{REF}^*)_{\text{MLO}} - \Delta T_{\text{adj}}(\text{S2}^* - \text{REF}^*)_{\text{fSST}}$$

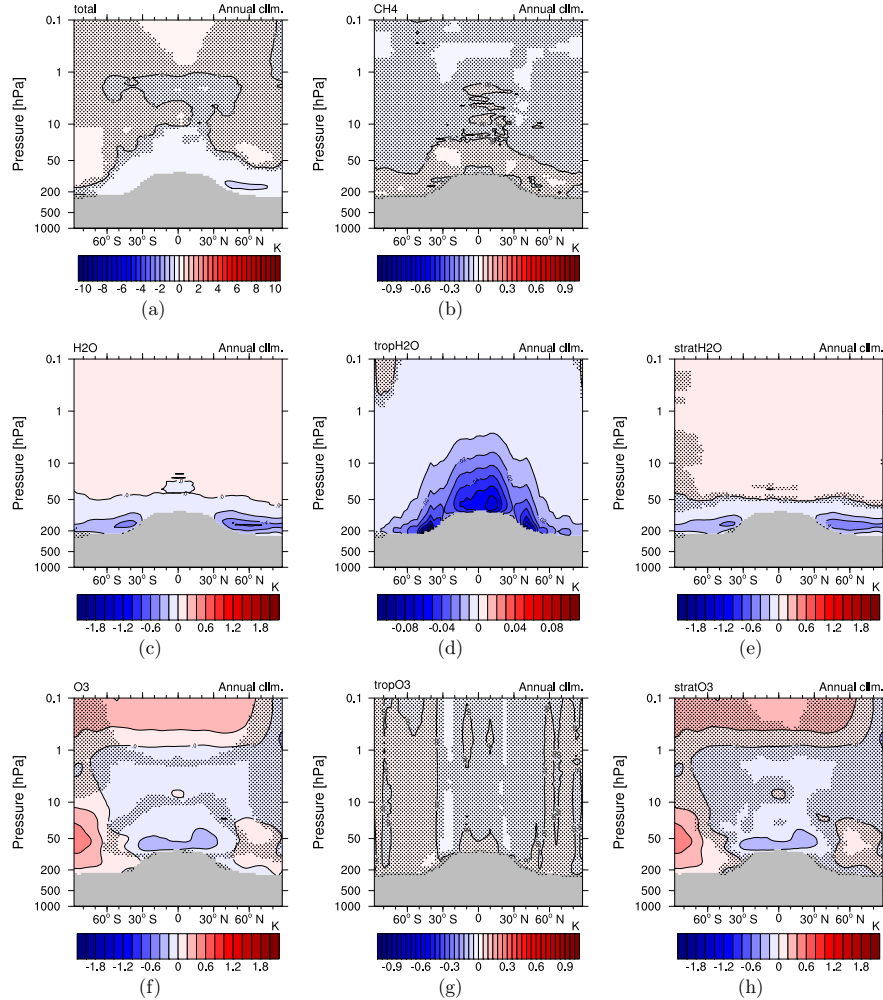


Figure S10. Difference between stratospheric temperature adjustment in simulations S2 MLO and S2 fSST ($2 \times \text{CH}_4$) radiatively induced by individual species changes: (a) CH_4 , H_2O and O_3 combined, (b) CH_4 , (c) H_2O , (d) tropospheric H_2O only, (e) stratospheric H_2O only (SWV), (f) O_3 , (g) tropospheric O_3 only and (h) stratospheric O_3 only. Note the different colour bars in panels (a), (b), (d) and (g).

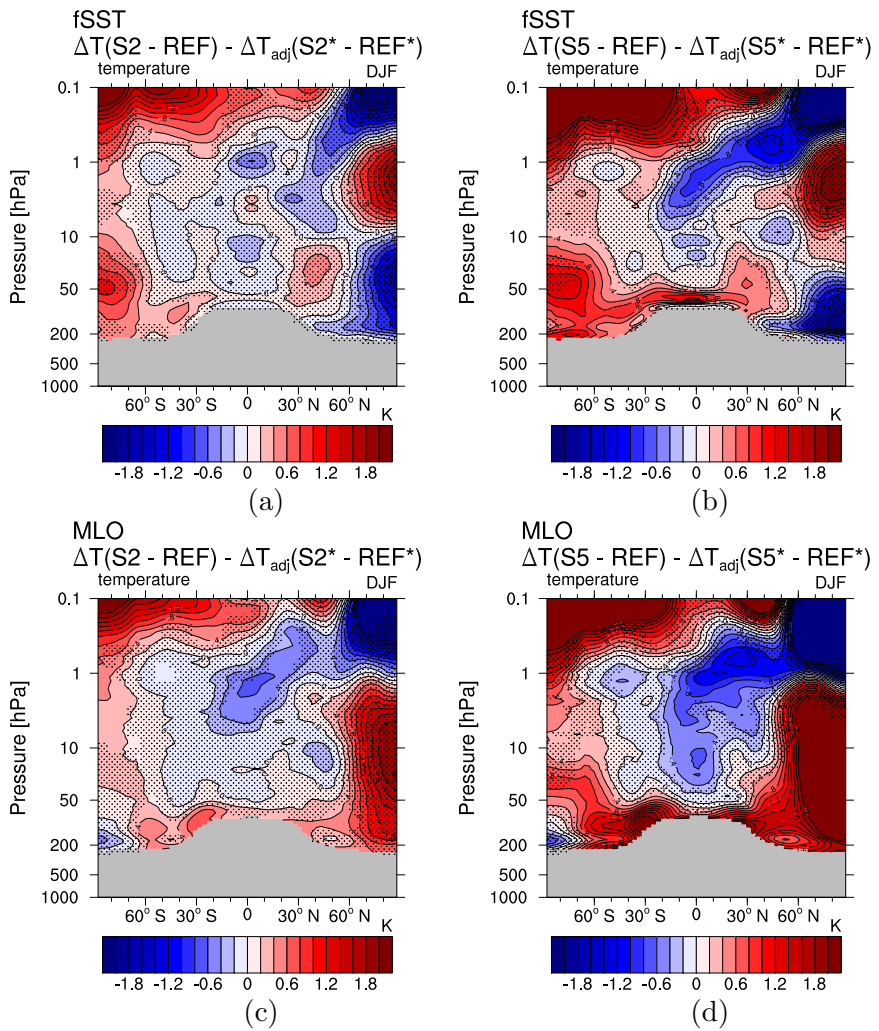


Figure S11. Dynamical temperature response effect for season DJF of the simulations (a) S2 fSST, (b) S5 fSST, (c) S2 MLO, (d) S5 MLO. The dynamical effect is calculated as the difference between the temperature response in the regular simulations ($\Delta T(\text{SX}-\text{REF})$ with X either 2 or 5) and the sum of the individual contributions of CH_4 , H_2O and O_3 to the stratosphere adjusted temperatures ($\Delta T_{\text{adj}}(\text{SX}^*-\text{REF}^*)$ with X either 2 or 5).

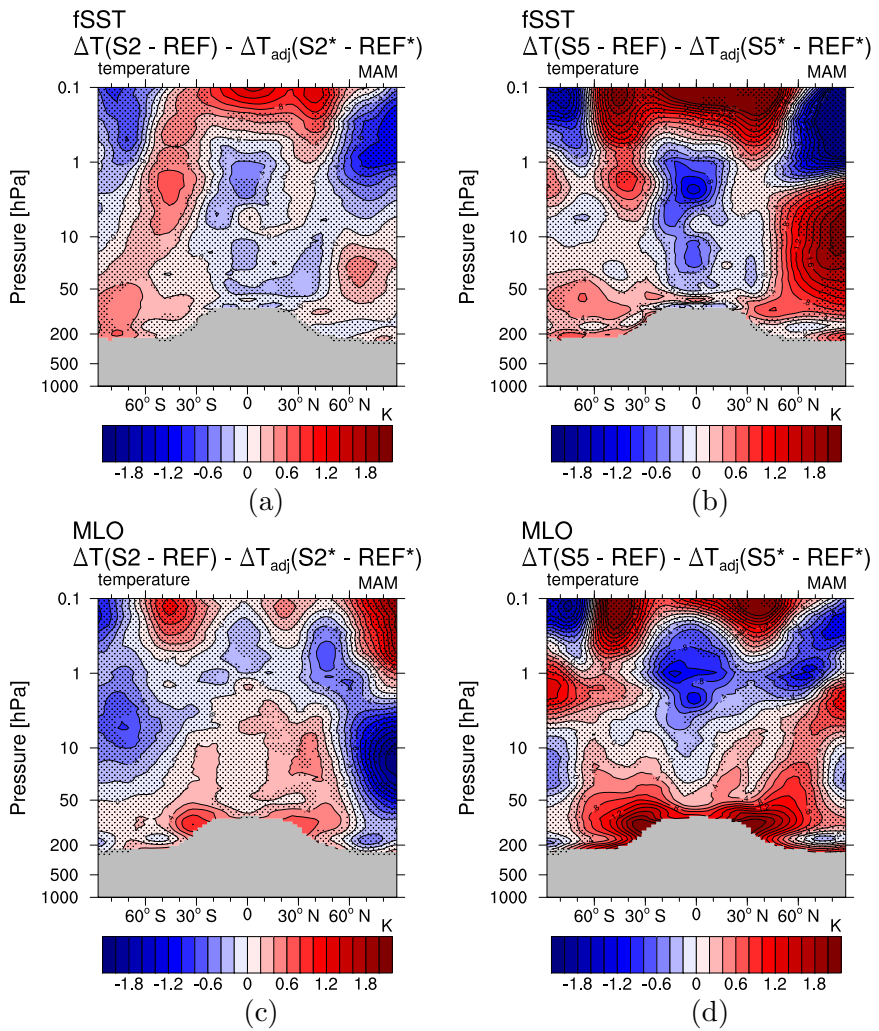


Figure S12. Dynamical temperature response effect for season MAM of the simulations (a) S2 fSST, (b) S5 fSST, (c) S2 MLO, (d) S5 MLO. The dynamical effect is calculated as the difference between the temperature response in the regular simulations ($\Delta T(SX\text{-REF})$ with X either 2 or 5) and the sum of the individual contributions of CH_4 , H_2O and O_3 to the stratosphere adjusted temperatures ($\Delta T_{\text{adj}}(SX^*\text{-REF}^*)$ with X either 2 or 5).

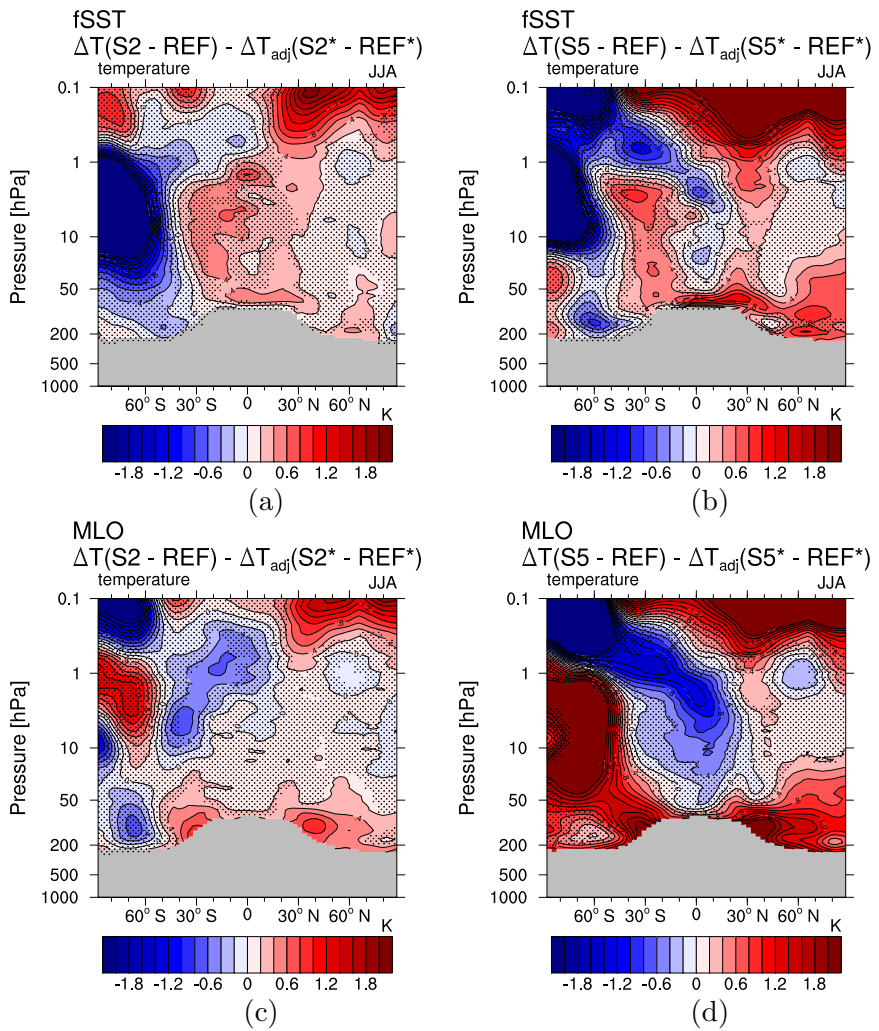


Figure S13. Dynamical temperature response effect for season JJA of the simulations (a) S2 fSST, (b) S5 fSST, (c) S2 MLO, (d) S5 MLO. The dynamical effect is calculated as the difference between the temperature response in the regular simulations ($\Delta T(\text{SX-REF})$ with X either 2 or 5) and the sum of the individual contributions of CH_4 , H_2O and O_3 to the stratosphere adjusted temperatures ($\Delta T_{\text{adj}}(\text{SX}^*-\text{REF}^*)$ with X either 2 or 5).

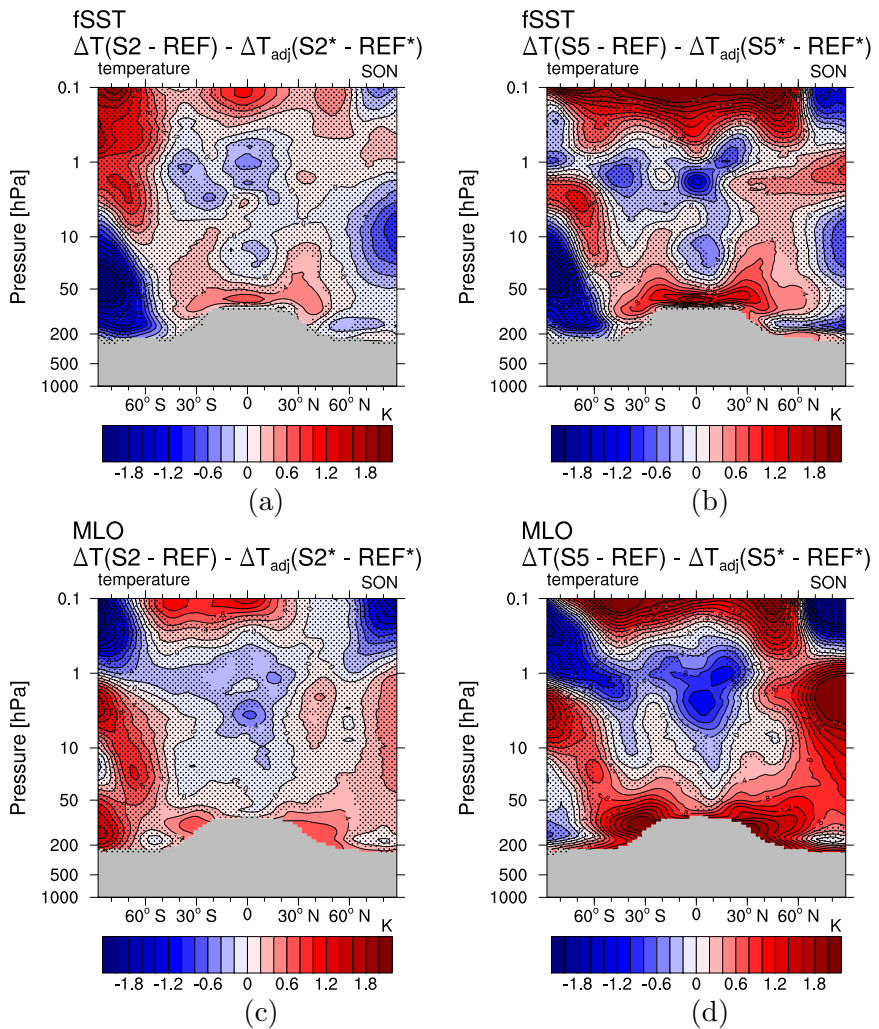


Figure S14. Dynamical temperature response effect for season SON of the simulations (a) S2 fSST, (b) S5 fSST, (c) S2 MLO, (d) S5 MLO. The dynamical effect is calculated as the difference between the temperature response in the regular simulations ($\Delta T(SX\text{-REF})$ with X either 2 or 5) and the sum of the individual contributions of CH_4 , H_2O and O_3 to the stratosphere adjusted temperatures ($\Delta T_{\text{adj}}(SX^*\text{-REF}^*)$ with X either 2 or 5).

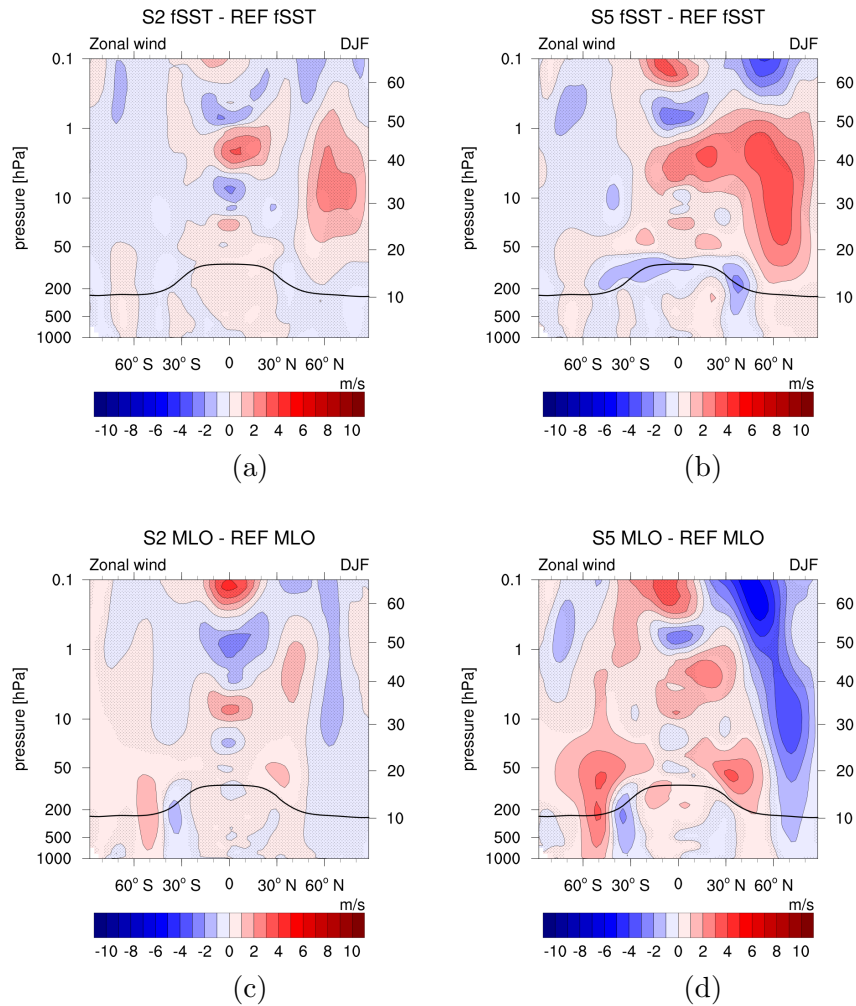


Figure S15. Absolute differences of zonal wind for season DJF of the sensitivity simulations (a) S2 fSST, (b) S5 fSST, (c) S2 MLO, (d) S5 MLO and their respective reference in m s^{-1} . Non-stippled areas are significant on the 95 % confidence level according to a two sided Welch's test. The solid black line indicates the climatological tropopause height of REF MLO.

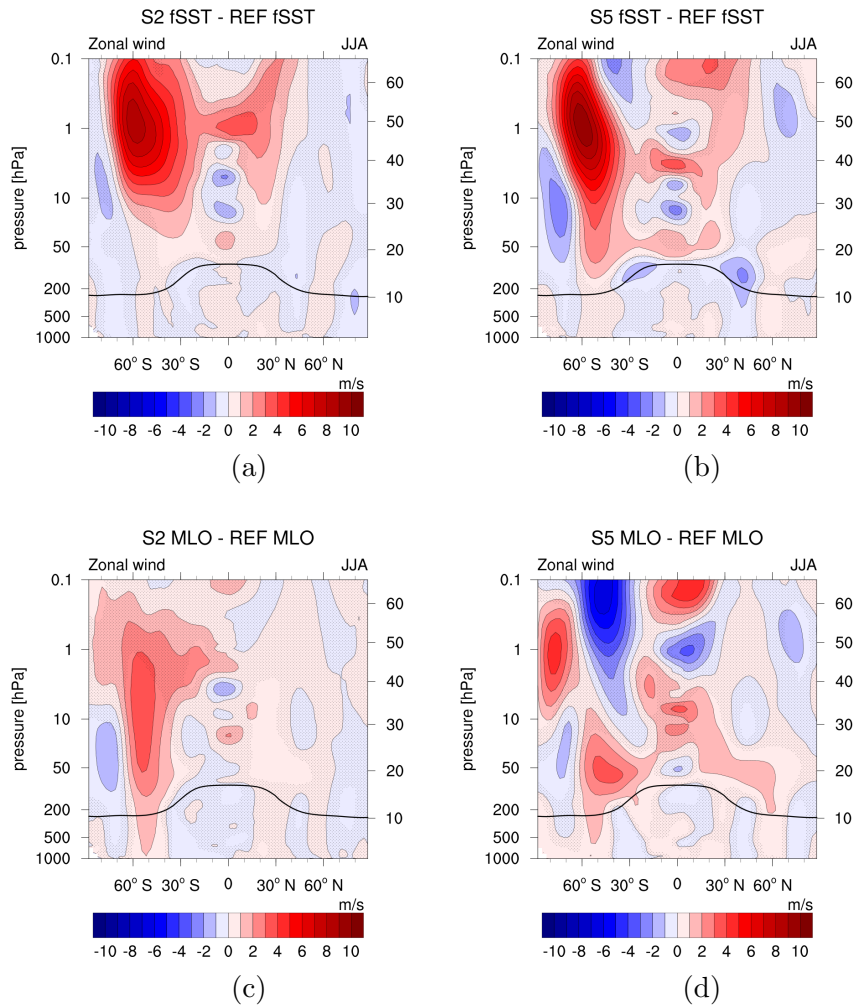


Figure S16. Absolute differences of zonal wind for season JJA of the sensitivity simulations (a) S2 fSST, (b) S5 fSST, (c) S2 MLO, (d) S5 MLO and their respective reference in m s^{-1} . Non-stippled areas are significant on the 95 % confidence level according to a two sided Welch's test. The solid black line indicates the climatological tropopause height of REF MLO.

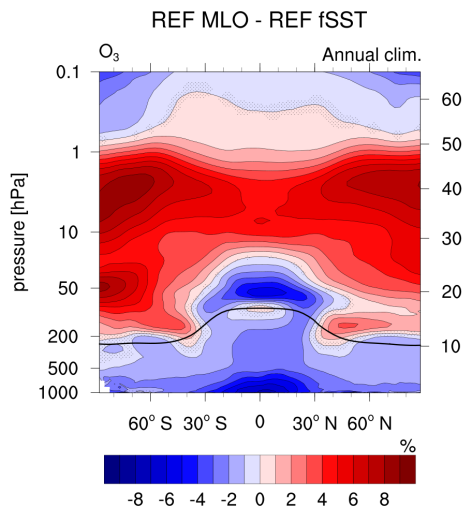


Figure S17. Relative differences of the annual zonal mean O_3 mixing ratio of REF MLO with respect to REF fSST in %. Non-stippled areas are significant on a 95 % confidence level according to a two sided Welch's test. The solid black line indicates the climatological tropopause height of the REF MLO.

Table S1. List of reactions, for which reaction coefficients changed from MESSy version 2.52 (fSST) to MESSy version 2.54.0 (MLO) in submodel Module Efficiently Calculating the Chemistry of the Atmosphere (MECCA; Sander et al. (2011a)).

Reaction	Reference for Reaction Rate Coefficient fSST	MLO
$\text{HO}_2 + \text{HO}_2 \rightarrow \text{H}_2\text{O}_2 + \text{O}_2$	Christensen et al. (2002), Kircher and Sander (1984)	Burkholder et al. (2015)
$\text{NO}_3 + \text{NO}_2 \rightarrow \text{N}_2\text{O}_5$	Sander et al. (2011b)	Burkholder et al. (2015)
$\text{N}_2\text{O}_5 \rightarrow \text{NO}_3 + \text{NO}_2$		
$\text{NO}_2 + \text{HO}_2 \rightarrow \text{HNO}_4$	Sander et al. (2011b)	Burkholder et al. (2015)
$\text{HNO}_4 \rightarrow \text{NO}_2 + \text{HO}_2$		
$\text{ClO} + \text{ClO} \rightarrow \text{Cl}_2\text{O}_2$	Atkinson et al. (2007)	Burkholder et al. (2015)
$\text{Cl}_2\text{O}_2 \rightarrow \text{ClO} + \text{ClO}$	Atkinson et al. (2007), Sander et al. (2011b)	
$\text{N}_2\text{O} + \text{O}^{(\text{lD})} \rightarrow 1.0 \text{ LossO}_3\text{O} + 1. \text{ LossO}_3 + 2 \text{ NO}$	Sander et al. (2011b)	Burkholder et al. (2015)
$\text{N}_2\text{O} + \text{O}^{(\text{lD})} \rightarrow 1.0 \text{ LossO}_3\text{O} + 1. \text{ LossO}_3 + \text{N}_2 + \text{O}_2$		
$\text{ClO} + \text{CH}_3\text{O}_2 \rightarrow 1.0 \text{ LossO}_3\text{Cl} + 1. \text{ LossO}_3 + \text{HO}_2 + \text{Cl} + \text{HCHO}$	Sander et al. (2011b)	Burkholder et al. (2015)
$\text{CH}_3\text{Cl} + \text{OH} \rightarrow 1.0 \text{ ProdLCl} + \text{LCARBON} + \text{H}_2\text{O} + \text{Cl}$	Sander et al. (2011b)	Burkholder et al. (2015)
$\text{CH}_3\text{CCl}_3 + \text{O}^{(\text{lD})} \rightarrow 3.0 \text{ ProdLCl} + 1.0 \text{ LossO}_3\text{Cl} + 1. \text{ LossO}_3 + 2 \text{ LCARBON} + \text{OH} + 3 \text{ Cl}$	extrapolation from reactions with CH_3CF_3 , CH_3CClF_2 and $\text{CH}_3\text{CCl}_2\text{F}$ from Sander et al. (2006)	Burkholder et al. (2015)
$\text{CH}_3\text{Br} + \text{OH} \rightarrow 1.0 \text{ ProdLBr} + \text{LCARBON} + \text{H}_2\text{O} + \text{Br}$	Sander et al. (2011b)	Burkholder et al. (2015)
$\text{CHBr}_3 + \text{OH} \rightarrow 3.0 \text{ ProdSBr} + \text{LCARBON} + \text{H}_2\text{O} + 3 \text{ Br}$	Sander et al. (2011b)	Burkholder et al. (2015)
$\text{CH}_2\text{ClBr} + \text{OH} \rightarrow 1.0 \text{ ProdSBr} + \text{LCARBON} + \text{LCHLORINE} + \text{H}_2\text{O} + \text{Br}$	Sander et al. (2011b)	Burkholder et al. (2015)
$\text{HNO}_3 + \text{OH} \rightarrow 1. \text{ ProdO}_3 + \text{H}_2\text{O} + \text{NO}_3$	Sander et al. (2011b)	Dulitz et al. (2018)

References

- Atkinson, R., Baulch, D. L., Cox, R. A., Crowley, J. N., Hampson, R. F., Hynes, R. G., Jenkin, M. E., Rossi, M. J., and Troe, J.: Evaluated kinetic and photochemical data for atmospheric chemistry: Volume III – gas phase reactions of inorganic halogens, *Atmos. Chem. Phys.*, 7, 981–1191, <https://doi.org/10.5194/acp-7-981-2007>, <https://www.atmos-chem-phys.net/7/981/2007/>, 2007.
- 5 Burkholder, J. B., Sander, S. P., Abbott, J. P. D., Barker, J. R., Huie, R. E., Kolb, C. E., Kurylo, M. J., Orkin, V. L., Wilmouth, D. M., and Wine, P. H.: Chemical Kinetics and Photochemical Data for Use in Atmospheric Studies, Evaluation No. 18, JPL Publication 15-10, Jet Propulsion Laboratory, <http://jpldataeval.jpl.nasa.gov/>, 2015.
- Christensen, L. E., Okumura, M., Sander, S. P., Salawitch, R. J., Toon, G. C., Sen, B., Blavier, J.-F., and Jucks, K. W.: Kinetics of $\text{HO}_2 + \text{HO}_2 \rightarrow \text{H}_2\text{O}_2 + \text{O}_2$: Implications for Stratospheric H_2O_2 , *Geophys. Res. Lett.*, 29, 13–1–13–4, <https://doi.org/10.1029/2001GL014525>, 2002.
- 10 Dulitz, K., Amedro, D., Dillon, T. J., Pozzer, A., and Crowley, J. N.: Temperature-(208–318 K) and pressure-(18–696 Torr) dependent rate coefficients for the reaction between OH and HNO_3 , *Atmos. Chem. Phys.*, 18, 2381–2394, <https://doi.org/10.5194/acp-18-2381-2018>, 2018.
- Kircher, C. C. and Sander, S. P.: Kinetics and mechanism of HO_2 and DO_2 disproportionations, *J. Phys. Chem.*, 88, 2082–2091,
- 15 <https://doi.org/10.1021/j150654a029>, <https://doi.org/10.1021/j150654a029>, 1984.
- Rayner, N. A., Parker, D. E., Horton, E. B., Folland, C. K., Alexander, L. V., Rowell, D. P., Kent, E. C., and Kaplan, A.: Global analyses of sea surface temperature, sea ice, and night marine air temperature since the late nineteenth century, *J. Geophys. Res.-Atmos.*, 108, <https://doi.org/10.1029/2002JD002670>, 4407, 2003.
- Sander, R., Baumgaertner, A., Gromov, S., Harder, H., Jöckel, P., Kerkweg, A., Kubistin, D., Regelin, E., Riede, H., Sandu, A., Taraborrelli, D., Tost, H., and Xie, Z.-Q.: The atmospheric chemistry box model CAABA/MECCA-3.0, *Geosci. Model Dev.*, 4, 373–380, <https://doi.org/10.5194/gmd-4-373-2011>, 2011a.
- Sander, S. P., Friedl, R. R., Golden, D. M., Kurylo, M. J., Moortgat, G. K., Keller-Rudek, H., Wine, P. H., Ravishankara, A. R., Kolb, C. E., Molina, M. J., Finlayson-Pitts, B. J., Huie, R. E., and Orkin, V. L.: Chemical Kinetics and Photochemical Data for Use in Atmospheric Studies, Evaluation No. 15, JPL Publication 06-2, Jet Propulsion Laboratory, <http://jpldataeval.jpl.nasa.gov>, 2006.
- 25 Sander, S. P., Abbott, J., Barker, J. R., Burkholder, J. B., Friedl, R. R., Golden, D. M., Huie, R. E., Kolb, C. E., Kurylo, M. J., Moortgat, G. K., Orkin, V. L., and Wine, P. H.: Chemical Kinetics and Photochemical Data for Use in Atmospheric Studies, Evaluation No. 17, JPL Publication 10-6, Jet Propulsion Laboratory, <https://doi.org/10.1002/kin.550171010>, <http://jpldataeval.jpl.nasa.gov/>, 2011b.